CFA/VISHNO 2016

A Three-Dimensional Numerical Study of Laminar Reciprocating Flow in a Square Thermoacoustic Stack

A. Abdel-Rahman, W. Abdelfattah et M. Fouad

Dept. of The Mechanical Power Engineering, Cairo University, Cairo University Rd., 12613 Giza, Égypte
ahmedibrahim@aucegypt.edu

The thermoviscous behavior of the oscillating gas within the porous medium of a thermoacoustic refrigerator enables the conversion of sound into heat in the process of typical standing thermoacoustic refrigeration systems. Several nonlinear mechanisms, such as harmonics generation, self-induced streaming and possible turbulence, cause complicated flow behavior and influence the performance of such devices. Few analytical and numerical approximations describe the flow field and the energy flux density in standing devices comprising stacks of parallel plates, but almost no 3-D simulation has been developed that models the large-amplitude excitations and enables the prediction of the oscillating-flow behavior within a porous medium made of square channels. Here, we build on existing effort and report a computational fluid dynamics analysis of a Helium-filled half-wavelength thermoacoustic refrigerator. The finite volume method is used, and the solid and gas domains are represented by large numbers of hexahedral elements. The calculations assume a 3-D periodic cell structure to reduce the computational cost and apply the dynamic mesh technique to account for the adiabatically oscillating wall boundaries. The simulation uses an implicit time integration of the full unsteady compressible flow equations along with the conjugate heat transfer algorithm. A typical run involves a million of computational cells, whereas the working frequency and the applied drive ratio are 592.5 Hz and 1.5%, respectively. The stationary system response is predicted and the numerical values are compared to theory. The results show good agreement with theoretical behavior in the linear regime of drive ratios and up to 2% while a maximum cooling effect of 10 degrees is captured at the optimum stack position. The relative importance of the different thermal mechanisms, involved within and around the stack, is discussed and the existence of nonlinear phenomenon such as streaming is demonstrated.

1   Introduction

A typical standing-wave thermoacoustic refrigerator (TAR) consists of a long resonator that is usually filled with an inert gas, a porous medium called 'Stack' and two heat exchangers. The stack of a standing-wave refrigerator is usually short and made of ceramic material, whereas the resonator is closed at one end and bounded by a loudspeaker at the other end, thus, allowing the propagation of a half-wavelength acoustic excitation. The hot and cold heat exchangers are made of copper to provide efficient heat transfer between the working inert gas and the external heat source and sink respectively. TARs are interesting because they have no moving parts, unlike conventional refrigerators, and almost no environmental impact exists as they rely on the conversion of acoustic and heat energies. Their fabrication process is rather simpler and sizes span wide variety of length scales.

In typical low-pressure excitation systems, the thermoacoustic behavior is dominated by the 1-D linear theory. However, practical systems fall into the high-pressure regime of acoustic excitation, where non-linear behavior is dominant. The following recent studies showed substantial deviation of most cooling curves from the linear theory. They rather focused on modeling thermoacoustic devices to help predict the general performance, capture the thermal and viscous flow losses in the device, and define key variables affecting the design considerations and system optimization, such as stack porosity, size and location, working gas and appropriate operating mean pressure.

Cao et al. [1] was the first to construct a first-order temporal and spatial discretization scheme to solve for the time-averaged energy flux density in the gas. In their model, the stack was represented by short (compared with the particle displacement length) isothermal parallel plates. Cao's attempt was followed by the significant effort of Worlikar et al. [2, 3] who considered the low-Mach number approximation of the full Navier-Stokes equations and solved the streamfunction-vorticity equation. They were able to successfully reduce the full computational domain into a single periodic thermoacoustic couple. Although limited to two-dimensional analysis, short stack lengths and constant

gas properties, their approach was then traced in similar fashion by other recent workers, such as Blanc-Benon et al. [4]. Blanc-Benon performed a particle image velocimetry (PIV) measurements of the flow field and reported close agreement with the low-Mach number simulation results.

Ishikawa and Mee [5] extended Cao analysis to longer plates and investigated the effects of plate spacing using the PHOENICS finite-volume method, however, their single-precision calculations caused significant energy imbalances and restricted the overall accuracy in their heat fluxes results. Latter, Marx and Blanc-Benon [6, 7] considered the time-averaged velocity field above the stack plate and observed the acoustic flow streaming above the plate. They further identified the minimum plate length, as compared to the particle displacement, necessary for the generated temperature harmonics to get displayed above the entire plate surface. Although accurate, this model is too expensive computationally to limit its applicability to devices operating at high-frequency of 20 kHz, which is useful for miniaturization purposes.

Zoontjens et al. [8] was the first to implement a FLUENT model to simulate the flow and energy fields in a TAR couple of non-zero thickness at a wide range of drive ratio (1.7%-8.5%) and 200 Hz operating frequency. They assumed symmetric computational domain and investigated the time-averaged heat transfer through the stack material. Their model however used a first-order discretization scheme which in turn affected the accuracy of their numerical results. This was recently followed by the work of Tasnim and Fraser [9] who introduced a two-dimensional model using the STAR-CD finite volume solver. He assumed a periodic thermoacoustic couple and described the laminar-flow and thermal fields at low drive ratio of 0.7%.

To our knowledge, no 3-D simulation has been developed that directly models the large-amplitude excitations of standing TARs. Building on existing effort [10], the objective of the present work is to extend the two-dimensional analysis of standing thermoacoustic couples into three-dimensional simulation of the oscillating-flow behavior within a porous medium made of square channels. Next, to investigate the thermoviscous interactions along the stack and at the
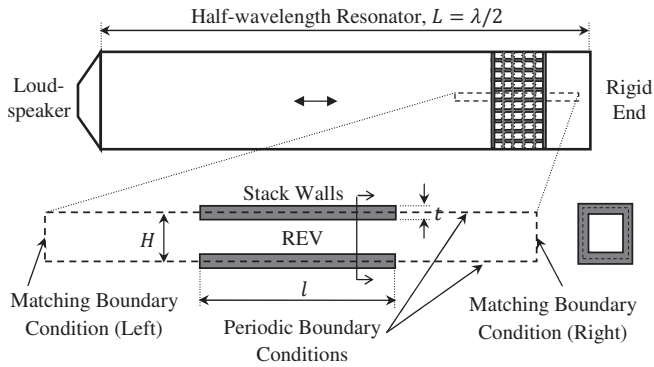
FIGURE 1 – Schematic of the thermoacoustic refrigerator is shown on top. Bottom : The representative element volume REV is drawn with a couple of periodic surfaces along with an acoustically-matching adiabatic boundary conditions imposed at both ends (the edge length of the square pore is $h = H - 2t$).

stack ends, and to evaluate the existence of non-linear phenomenons, such as DC-streaming.

2 Numerical Model Setup

For the sake of simulation and model validation, the current geometry and operating conditions follow the experimental setup of Lotton et al. [11] except for the stack length and the operating gas. The system is excited with an acoustic frequency of 592.5 Hz and acoustic pressure amplitude in the range from $250 - 2000$ Pa. The resonator has a square cross section and filled with Helium at atmospheric pressure and ambient temperature. The stack is made of cordierite (ceramic material) and consists of a large number of small square channels (600 CPSI), aligned with the direction of wave propagation. Here, each channel is 10-mm-in-length and has a transversal width h of 0.92 mm and a wall thickness t of 0.12 mm. The numerical model is constructed such that the stack centre is positioned at a distance 140 mm from the resonator closed end. According to Lotton et al. [11], such stack position corresponds to the maximum cooling effect.

It is unreasonable to model the entire domain of the thermoacoustic resonator and the stack. Therefore, an element volume that includes one gas channel is chosen to represent the oscillating-flow behavior within the stack and at the stack ends, as shown in Fig. 1. To account for the rest of the domain in the cross-streamwise direction, the element volume is enclosed by a couple of periodic boundaries. The 3-D computational domain is then allowed to extend in the axial direction with a total length of 4.64 times the stack length l. An acoustically matching boundary condition is thus imposed at both left and right ends, assuming an ideal acoustic wave propagation. The layering dynamic meshing technique is used for this purpose.

Figure 2 presents the domain meshing in the transversal and longitudinal directions. The domain is carefully discretized to properly capture the thermoviscous interactions of the oscillating-flow with the stack walls and to maintain grid-independent system response. The flow is assumed laminar. Such flow approximation will be elaborated in the results section through the specification of
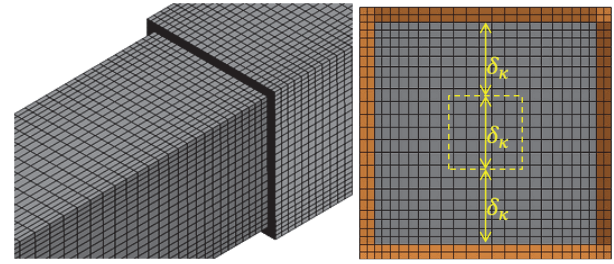
FIGURE 2 – The left figure presents the 3-D meshing of the computational gas domain, as spanned from inside the stack to the outside of it. The solid mesh is suppressed for clarity. However, the right plot shows a side view -transversal cut- of the whole computational domain (Inset : $\delta_\kappa \approx 0.31$ mm). Here, the yellow frame represents the solid stack, while the gray structured mesh corresponds to the gas domain with a minimum cell size of 0.03 mm and a maximum of 0.05 mm.

two key parameters [12, 13] : the dimensionless frequency parameter $h^2\omega/\nu$ (Also, referred as the Womeresley number for circular pipe) and the flow Reynolds number $Re = \hat{U}\delta_\nu/\nu$, based on the amplitude of the cross-sectional mean-velocity variation $\hat{U}$ and the viscous diffusion thickness $\delta_\nu = \sqrt{2\nu/\omega}$. Here, ν and ω are the gas viscous diffusivity and the angular frequency, respectively.

In the transversal direction, the mesh is distinguished into two concentric regimes, depth of each corresponds to the thermal diffusion thickness $\delta_\kappa = \sqrt{2\alpha/\omega}$, where α is the gas thermal diffusivity. In the first regime, the flow experiences steep velocity and temperature gradients, therefore, eight computational cells are enforced to capture the flow behavior very near to the wall. Less steep gradients are expected in the second regime, thus, five larger cells are assumed sufficient since this regime lies in the stack core, where poor transversal fluctuation in the flow properties generally evolves. In the longitudinal direction, a structured hexahedral mesh is maintained such that the cell height varies gradually and smoothly from one to five times the cell width throughout the entire domain, as indicated in Fig. 2(Left). For instance, the resulting total number of cells is around 2×10^5.

The present analysis uses the ANSYS FLUENT second-order upwind implicit-time algorithm CFD solver with the conjugate heat transfer algorithm along with a second-order formulation for the temporal discretization. The high-accuracy pressure staggering scheme (PRESTO) is enabled as the pressure interpolation scheme at the computational element faces, while the pressure-implicit with splitting of operators (PISO) pressure-velocity coupling scheme is applied. Double-precision parallel computation is essential to this analysis, therefore, the computational domain is divided into eight partitions and each simulation run is performed on an eight-core workstation and consumes a CPU time of about a month to reach its quasi-stationary response. A fixed time step is chosen 1/120 of the acoustic period and convergence is claimed when the absolute variation in each of the flow quantities (residuals) is less than 10^{-4} (convergence criteria) in any two successive iterations.

A typical transient behavior of the present computational model is shown in Fig. 3 at drive ratio of 2%. As the simulation proceeds, heat is being extracted from the stack cold end, carried by the introduced acoustic oscillations
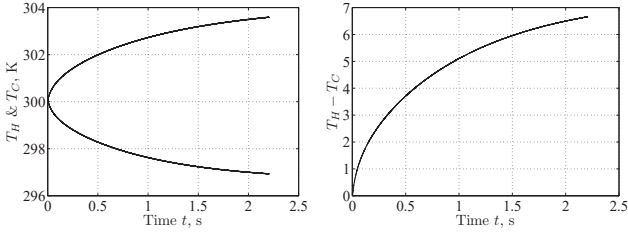
FIGURE 3 – Temperature history at the stack ends (Left) and variation of the temperature difference $\Delta T = T_H - T_C$ at 2% drive ratio (Right).
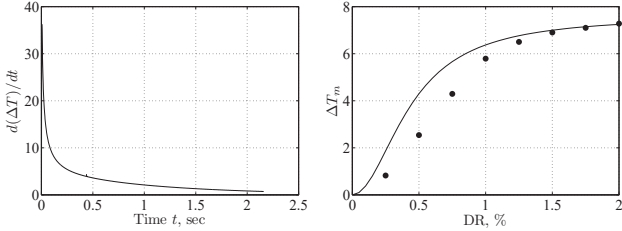
FIGURE 4 – The time rate of change of gas temperature at $DR = 2\%$ is plotted in the left figure, while a comparison of the resulting ΔT_m with theory, following Eq. 7, is indicated in the right plot.

through the working gas and pumped into the stack hot end. This causes an increase in the temperature of the stack hot end (near the resonator rigid end or the velocity node), while the temperature decreases at the stack cold end. The variation with time of the temperature difference ΔT along with its rate of change are illustrated in Fig. 4. In support to the work of Worlikar et al. [3], the present temperature difference increases rapidly in the few early time steps, then decreases sharply with a noticeable exponential decay to asymptotically approach its steady-state value at sufficiently large simulation time. In the present simulation run, the calculations are allowed to proceed till the time rate of change drops to less than 2% of its initial value. Numerical values of $d(\Delta T)/dt$ at large times are next extrapolated through an exponentially-decaying fitting process to yield the exact steady-state value of the ANSYS's predicted temperature difference.

3   Model Validation

The theoretical framework of both heat and work flows within a thermoacoustic couple in the short stack approximation has been extensively reviewed in literature [14, 15], whereas fewer works were reported for stacks having arbitrarily shaped pore cross sections. Arnott [16] derived the time-averaged thermoacoustic heat flow equation due to hydrodynamic transport for square pores stack geometry, as follows :

$$\overline{\dot{Q}}(x) = \frac{AP_L^2 \sin(2kx)}{4\rho a(1+\sigma)} \, \mathfrak{I}\left(\frac{F^*(\lambda_\kappa)}{F(\lambda_\nu)}\right)\left(1 - \Gamma \frac{\mathfrak{I}[F(\lambda_\kappa) + \sigma F^*(\lambda_\nu)]}{\mathfrak{I}[F(\lambda_\kappa)F(\lambda_\nu))](1+\sigma)}\right)$$

(1)

where,

$$\Gamma = \frac{dT_m}{dx}\frac{C_p \tan(2kx)}{\omega \Omega a}$$

(2)

Here, the overbar denotes the time-average component of the second-order heat flow $\dot{Q}$, whereas $\mathfrak{I}$ refers to the

imaginary part of its argument. A and Ω refer to the resonator cross-sectional area and the stack porosity, while x indicates the axial position, measured from the resonator closed end. The properties ρ, C_p and σ represent the density, specific heat and Prandtl number of the working gas, respectively. P_L, a and k correspond to the dynamic pressure amplitude at the resonator closed end, the speed of sound and the wave number, respectively. dT_m/dx is the mean temperature gradient along the stack.

Equation 1 describes the heat flow in terms of the geometrical thermoviscous functions $F(\lambda_\nu)$ and $F(\lambda_\kappa)$ and their complex conjugates $F^*(\lambda_\nu)$ and $F^*(\lambda_\kappa)$. According to Arnott [16], they are defined as :

$$F(\lambda_{\nu,\kappa}) = \frac{64}{\pi^4} \sum_{m,n \text{ odd}} \frac{1}{m^2 n^2 Y_{mn}(\lambda_{\nu,\kappa})}$$

(3)

$$Y_{mn}(\lambda_{\nu,\kappa}) = 1 + \imath \pi^2 (m^2 + n^2)/(4\lambda_{\nu,\kappa}^2)$$

(4)

$$\lambda_{\nu,\kappa} = 2\sqrt{2}\, r_h/\delta_{\nu,\kappa}$$

(5)

The dimensionless shear wave number λ_ν is defined as the ratio of the pore hydraulic radius r_h to the gas viscous diffusion thickness δ_ν. Similarly, λ_κ corresponds to the thermal diffusion thickness δ_κ. In the present work, the first 16 terms of the summation series were found sufficient to solve for the real and imaginary components of the thermoviscous functions.

To further proceed with the theoretical estimation of the developed temperature gradient along the stack at no load - Heat exchangers were not included in the experimental setup of Lotton et al. [11] for simplicity-, the time-averaged heat transferred in the oscillating-gas due to the thermoacoustic heat-pumping effect from the cold to the hot stack ends must be balanced, at dynamic equilibrium, with the diffusive conduction down the yet-generated temperature gradient through both the gas and solid domains. In a similar process to that followed by Wheatley et al. [15], the theoretical amount of heat transfer, presented in Eq. 1, can be expressed as a function of the gas and solid thermal conductivities K_g and K_s, respectively, as follows :

$$\overline{\dot{Q}}(x) = K_{\text{eff}}A\frac{dT_m}{dx} = (\Omega K_g + (1-\Omega)K_s)A\frac{dT_m}{dx}$$

(6)

Substituting Eq. 1 into Eq. 6, solving for dT_m/dx, and then integrating with respect to the axial direction over the stack length l yields the temperature difference ΔT_m -Noting that in the short-stack approximation, the spatially-averaged components can be fairly replaced by their corresponding values at the stack center $\bar{x}$-

$$\Delta T_m \approx \frac{\frac{AP_L^2 l \sin(2k\bar{x})}{4\rho a(1+\sigma)} \, \mathfrak{I}\left(\frac{F^*(\lambda_\kappa)}{F(\lambda_\nu)}\right)}{K_{\text{eff}}A + \frac{AP_L^2 \sin(2k\bar{x})}{4\rho a(1+\sigma)} \, \mathfrak{I}\left(\frac{F^*(\lambda_\kappa)}{F(\lambda_\nu)}\right) \frac{\mathfrak{I}[F(\lambda_\kappa)+\sigma F^*(\lambda_\nu)]}{\mathfrak{I}[F(\lambda_\kappa)F(\lambda_\nu)](1+\sigma)} \frac{C_p \tan(2k\bar{x})}{\omega \Omega a}}$$

(7)

To validate the present numerical model, the theoretical values (Eq. 7) are plotted in Fig. 4 along with the predicted quasi-steady state temperature difference across the stack. Surprisingly, the results show better agreement with the linear theoretical behavior with the increase of the drive ratio and up to $DR = 2\%$. It is worth mentioning that the error gained during the estimation of the steady-state values ΔT_m using the exponentially-decaying fits decreases as the drive ratio gets higher. In addition to that, the discrepancies between the theoretical prediction and the present numerical
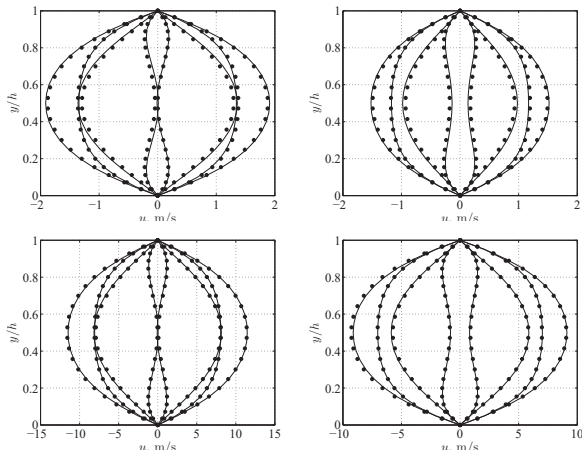
FIGURE 5 – Velocity Profiles at drive ratios 0.25% (Top) and 1.5% (Bottom), as compared to the Arnott's extended linear theory (Solid lines) for oscillating flow in square pores at an axial distance of $l/2$ from the stack cold end. The profiles are plotted at two different transversal sections of the gas square channel, corresponding to $0.25h$ and $0.5h$, respectively.

values at lower drive ratios is possibly due to typical numerical dissipation associated with the numerical upwind discretization scheme [17], considered by the ANSYS solver in the present simulation. Such losses are becoming remarkably higher as the drive ratio gets lower.

4 Results & Discussion

4.1 Axial Velocity Profiles

Through similar mathematical manipulation, the theoretical axial profiles of the reciprocating flow velocity for 45°-increments over one period are shown in Fig. 5 in comparison with the present numerical values for drive ratios 0.25% and 1.5%, respectively, and at two different depths to illustrate the three-dimensional flow behavior within the square pores. Nodal values of the axial velocity are first extracted from ANSYS solver and then passed to a specifically-developed MATLAB program for postprocessing. The profiles are plotted at $l/2$ with a peak axial velocity of 12 m/s at the stack centerline while opearting at $DR = 1.5\%$, whereas no sign of flow reversal is captured in the present prediction.

Furthermore, typical laminar flow oscillations are noticed at both drive ratios, and the system is clearly linear in the present simulation runs. To further demonstrate the propagation of laminar flow, both the dimensionless frequency parameter and the Reynolds numbers are estimated. For instance, at 1.5% drive ratio, the amplitude of the cross-sectional mean-velocity variation $\hat{U} \approx 8$ m/s. Thus, for a viscous penetration depth of $\delta_\nu \approx 0.26$ mm, the frequency parameter and Reynolds number are $h^2\omega/\nu \approx 25.4$ and $\hat{U}\delta_\nu/\nu \approx 16.74$, respectively. According to Hino et al.[13], these values are fairly low for a transition to turbulence to take place.
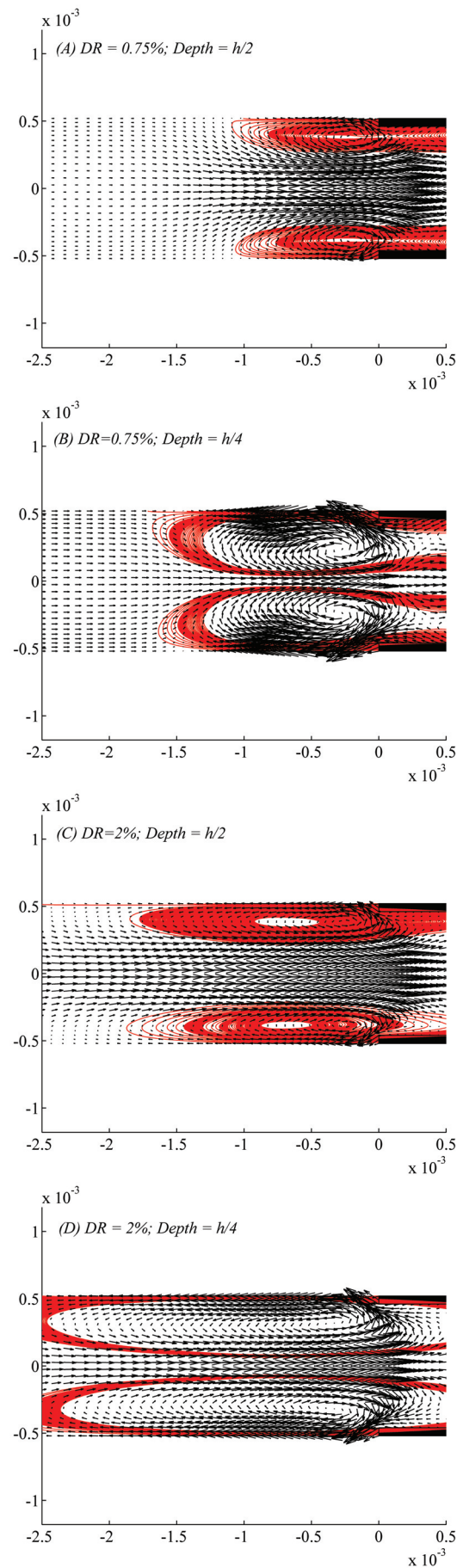
FIGURE 6 – Vector plots superimposing streamlines (Solid red lines) of the energy flux density at drive ratios of 0.75% (A & B) and 2.0% (C & D) over planes located 0.25 and 0.5 the channel width h in the transversal direction.

4.2 Energy Flux Density

A better description of the heat transport process from the stack cold end to the stack hot end is here introduced through the calculation of the time-averaged of the energy flux density over the last acoustic period. A specific user defined function is developed to record the instanteneous nodal values of the gas temperature, velocity and temperature gradients and thus, enable the calculation of the time-averaged (mean) components of the energy flux density, according to :

$$\overline{\mathbf{H}} = C_p \overline{\rho(T - T_m)\mathbf{u}} - K_g \overline{\nabla T} \qquad (8)$$

Further post-processing is achieved using a specific MATLAB program. Figure 6 shows the energy streamlines -superimposed by the vector plots- of the energy flux density for different drive ratios at different depths, as predicted in the present numerical simulation runs. Here, the time-averaged energy streamlines are plotted, such that their starting positions are located at the stack cold inner-surfaces and sides for the sake of visualization. It is clearly shown in figure that, because of the thermoacoustic heat pumping effect, the thermal energy is first extracted from the inner walls and sides at the cold end, swirls in an eddy-like motion till finds its straight-path through the gas along the stack to finally get rejected into the hot end.

Figures 6 (A&D) refer to the energy flux densities near the stack corners, as predicted over a plane located $0.25h$ away from the stack inner walls, while Figs. 6 (A&C) correspond to those fluxes calculated at the stack mid-plane ($0.5h$-deep). The plots are presented for the stack cold end for clarity. The vectors lengths are automatically scaled for visualization, whereas, the prediction reveals a maximum vector length of 123.89 and 672.82 W/m^2 at 0.75% and 2%, respectively.

The figures illustrate the existence of large-areas of recirculating mean energy fluxes, intensity of which increases by moving towards the stack corners, as particularly indicated in Figs. 6 (B&D). It is also observed that the axial extension of the recirculating zones closely correponds to the cross-sectional mean particle displacement $\hat{U}/\omega$, particularly at the stack corners. Furthermore, the energy fluxes calculated at the stack mid-plane are shown to be more concentrated rather than detached, as indicated by those plotted nearby the stack corners. Remarkably, such recirculating zones become not only significant as the drive ratio increases, but also exhibit longer recirculating pathlines before getting back into the stack. This is in part consistent with -and is possibly caused by- the induced non-zero mean DC-streaming and its associated vortical motion at the stack extremities, as reported by Marx et al. [6, 7], with similar dependence on the imposed drive ratio. This might in turn assume a significant contribution to the overall thermal energy losses. Interestingly, this is not supported by the above agreement of the mean temperature difference with theory at large drive ratios. It is therefore concluded that the Rott's linear theory still holds up to this limit.

5 Summary

A new three-dimensional finite-volume model is presented to examine the thermoviscous interactions between the oscillating-gas and the solid walls in a thermoacoustic stack made of square pores. The model enables us to investigate the temperature variation with time at the stack ends along with the evolving axial velocity profiles within the stack at different transversal planes. The mean (time-averaged) energy flux density is also calculated and presented in this study. In the present simulation runs, the predicted instantenous velocity profiles and the variation with the drive ratio of the estimated mean temperature difference ΔT_m between the stack ends show good agreement with the linear theory up to a drive ratio of 2%. Although clearly evident both at the stack extremities and within the stack, the behavior of the energy flux pathlines does not appear to substantially the resulting mean-temperature difference between the stack ends, particularly at drive ratio 2%.

Références

[1] N. Cao, J. R. Olson, G. W. Swift, S. Chen, Energy flux density in a thermoacoustic couple, The Journal of the Acoustical Society of America 99 (6) (1996) 3456–3464.

[2] A. S. Worlikar, O. M. Knio, Numerical simulation of a thermoacoustic refrigerator : I. unsteady adiabatic flow around the stack, Journal of Computational Physics 127 (2) (1996) 424 – 451.

[3] A. S. Worlikar, O. M. Knio, R. Klein, Numerical simulation of a thermoacoustic refrigerator : Ii. stratified flow around the stack, Journal of Computational Physics 144 (2) (1998) 299 – 324.

[4] P. Blanc-Benon, E. Besnoin, O. Knio, Experimental and computational visualization of the flow field in a thermoacoustic stack, Comptes Rendus Mécanique 331 (1) (2003) 17 – 24.

[5] H. Ishikawa, D. J. Mee, Numerical investigations of flow and energy fields near a thermoacoustic couple, The Journal of the Acoustical Society of America 111 (2) (2002) 831–839.

[6] D. Marx, P. Blanc-Benon, Computation of the mean velocity field above a stack plate in a thermoacoustic refrigerator, Comptes Rendus Mécanique 332 (11) (2004) 867 – 874.

[7] D. Marx, P. Blanc-Benon, Computation of the temperature distortion in the stack of a standing-wave thermoacoustic refrigerator, The Journal of the Acoustical Society of America 118 (5) (2005) 2993–2999.

[8] L. Zoontjens, C. Howard, A. Zander, B. Cazzolato, Numerical study of flow and energy fields in thermoacoustic couples of non-zero thickness, International Journal of Thermal Sciences 48 (4) (2009) 733 – 746.

[9] S. H. Tasnim, R. A. Fraser, Computation of the flow and thermal fields in a thermoacoustic refrigerator, International Communications in Heat and Mass Transfer 37 (7) (2010) 748 – 755.

[10] A. I. Abd El-Rahman, E. Abdel-Rahman, Computational fluid dynamics simulation of a thermoacoustic refrigerator, Journal of Thermophysics and Heat Transfer 28 (1) (2014) 78 – 86.

[11] P. Lotton, P. Blanc-Benon, M. Bruneau, V. Gusev, S. Duffourd, M. Mironov, G. Poignand, Transient temperature profile inside thermoacoustic refrigerators, International Journal of Heat and Mass Transfer 52 (21-22) (2009) 4986 – 4996.

[12] C. Fan, B.-T. Chao, Unsteady, laminar, incompressible flow through rectangular ducts, Zeitschrift für angewandte Mathematik und Physik ZAMP 16 (3) (1965) 351–360.

[13] M. Hino, M. Kashiwayanagi, A. Nakayama, T. Hara, Experiments on the turbulence statistics and the structure of a reciprocating oscillatory flow, Journal of Fluid Mechanics 131 (1983) 363–400.

[14] G. W. Swift, Thermoacoustic engines, The Journal of the Acoustical Society of America 84 (4) (1988) 1145–1180.

[15] J. Wheatley, T. Hofler, G. W. Swift, A. Migliori, An intrinsically irreversible thermoacoustic heat engine, The Journal of the Acoustical Society of America 74 (1) (1983) 153–170.

[16] W. P. Arnott, H. E. Bass, R. Raspet, General formulation of thermoacoustics for stacks having arbitrarily shaped pore cross sections, The Journal of the Acoustical Society of America 90 (6) (1991) 3228–3237.

[17] O. Zikanov, Essential Computational Fluid Dynamics, Wiley, 2010.